# ELASTODYNAMIC RECIPROCITY RELATIONS FOR WAVE SCATTERING BY FLAWS IN FIBER-REINFORCED COMPOSITE PLATES

W. KARUNASENA

Centre of Excellence in Engineered Fiber Composites, Faculty of Engineering and Surveying, University of Southern Queensland, Toowoomba, Queensland 4350, Australia.

Due to light weight, high performance and increased service life, fiber-reinforced composite materials are receiving wide attention as an advanced material in many branches of engineering. Structural integrity of composite structures is affected by the presence of flaws such as cracks and delaminations in the composite material. In this paper, elastodynamic reciprocity relations are developed for wave scattering by flaws when guided waves are allowed to propagate in fiber-reinforced composite plates. These relations are useful to check the accuracy of the numerical solution for the scattered wave field in ultrasonic non-destructive evaluation of flaws in composite plate-like structural elements. The classical elastodynamic reciprocity theorem is used to derive simple reciprocity relations for reflected and transmitted wave amplitudes and the corresponding energies associated with the wave modes in a plate with an arbitrary stacking sequence. The derived reciprocity relations are used to check the accuracy of the numerical solution for several example scattering problems.

*Keywords:* Reciprocity relations, Wave scattering, Composite plates, Cracks, Delaminations, Finite Elements, Reflection and transmission coefficients.

## 1. Introduction

In the last two decades, fiber-reinforced composite materials, specially fiber-reinforced plastics (abbreviated as FRPs), have been receiving wide attention in aerospace, civil and mechanical engineering applications due to their useful properties such as light weight, high strength, corrosion resistance and long term durability. A state-of-the-art-review of FRP composites for construction applications can be found in [1]. It is well known that structural integrity of facilities made from FRPs are severely affected by flaws such as cracks and delaminations developed within the FRP part of the structure. Guided elastic waves in plate-like composite parts possess characteristics that make them particularly useful for applications in non-destructive evaluation of flaws in composite structures. When excited at a particular location in a plate, guided waves can travel long distances along the plate and when they meet a flaw along their path, the waves start scattering. The scattered wave, which can travel long distances along the plate, will carry information about the size and location of the flaw,

thus providing an ultrasonic non-destructive means of inspection of an otherwise inaccessible area of the structure. Ultrasonic non-destructive evaluation methods heavily rely on the solution to the problem of wave scattering that happens at the flaw.

Obtaining closed-form solutions to even for simple wave scattering problems in composite plates is not practical if not impossible. Numerical methods for obtaining a solution to the scattered wave field are quite intricate and complicated, and as a result, the accuracy of a numerically obtained solution is questionable. One way of overcoming this problem is having some indicators based on sound theories to check the accuracy of the numerical solution. Two indicators used in the past are the satisfaction of elastodynamic reciprocity relations and the principle of energy conservation.

Chimenti [2] has published a comprehensive review of guided waves in composite plates and their use for non-destructive material characteristion. Datta [3] provided a detailed review of the theory of guided waves in composite plates and shells. Although a vast body of work on guided ultrasonic wave propagation in plates and shells now exists, relatively few studies have dealt with scattering of these waves by cracks and delaminations. Moreover, these few studies have been mostly confined to the problems of horizontally polarized shear (SH) waves and plane strain (two-dimensional) waves. The author and his co-workers [4] have investigated the two-dimensional wave scattering by a symmetric normal surface breaking crack in a cross-ply laminated plate by using a hybrid method which combines finite element method with wave function expansion procedure. In these work, authors have used the satisfaction of the reciprocity relations and the principle of energy conservation as checks for accuracy. The two checks serve as complementary to each other.

Recently, author [5] extended the hybrid method to provide a model analysis of scattering of a guided wave incident obliquely on a long symmetric surface breaking crack in a composite plate. The solution to this problem is the first step towards analyzing the general three-dimensional scattering in a composite plate. As mentioned in the previous paragraph for simple wave scattering problems, satisfaction of the reciprocity relations can be used as one of the two complementary checks for assessing the accuracy of the more complicated oblique wave scattering problem. The focus of this paper is to present the derivation of elastodynamic reciprocity relations for the scattering problem of a guided wave incident obliquely on a long flaw in a composite plate. The analysis is presented for a plate with an arbitrary stacking sequence where each ply can have an arbitrary fiber direction with respect to the global coordinate system. Numerical results for reciprocity relations are provided for four special cases – (i) scattering by a symmetric normal edge crack in a uni-directional fiber-reinforced homogeneous graphite-epoxy composite plate, (ii) scattering by a symmetric normal edge crack in an 8 layer graphite-epoxy cross-ply laminated plate, (iii) scattering by a thin planar crack

located at the fixed-end of a homogeneous isotropic plate. and (iv) scattering by a thin planar crack located at the fixed-end of a uni-directional fiber-reinforced composite plate.

## 2. Formulation

### 2.1 *Scattering problem*

Time harmonic wave scattering of a guided plate wave incident obliquely on a flaw in a composite plate as shown in Figure 1 is considered. The composite material in the plate is uni-axially fibre-reinforced within each layer (or ply or lamina) and possibly laminated with each ply having an arbitrary fibre-direction with respect to the global x-direction. Each layer lies on a plane parallel to x-y plane. It is assumed that all layers of the plate have equal thickness with transversely isotropic elastic properties. The flaw is located at x = 0 and is assumed to be very long (in comparison to the plate thickness) in y-direction. It has a constant cross-section in x-z plane. It is assumed that two faces of the plate z = 0 and z = H are stress free. Also, the flaw surface is assumed to be open with zero traction. Since the direction of the flaw (i.e. y-direction in this case), in general, is not known *a priori,* it is not always possible to excite the incident wave in the x-direction. Therefore, it is necessary to consider the general case where the incident wave is propagating at an arbitrary angle to the x-direction and the fiber direction is also at an arbitrary angle to global x-direction. Let the incident wave be a guided plate wave mode travelling at a direction making an angle $90^0 - \phi^{in}$ with the y-z plane and fibers be at an angle $\theta$ to the x-direction as shown in Figure 2.

When the incident wave mode strikes the flaw, mode conversion will happen and a scattered field consisting of reflected and transmitted plate wave modes will be generated. The aim of this work is to numerically quantify this scattered field and derive reciprocity relations applicable to converted modes for the purpose of checking the accuracy of the numerical solution for the scattered wave field. In general, the incident and the scattered wave field will have all three displacement components in the x, y, and z directions. Let u(x,y,z,t), v(x,y,z,t), and w(x,y,z,t) denote the displacement quantities in x, y, and z directions, respectively. Here t denotes time.

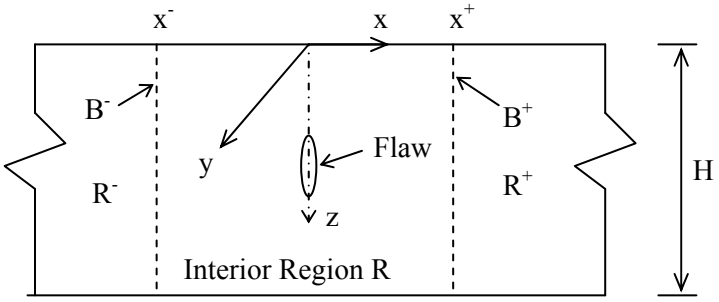


**Figure 1. Geometry of the Problem**

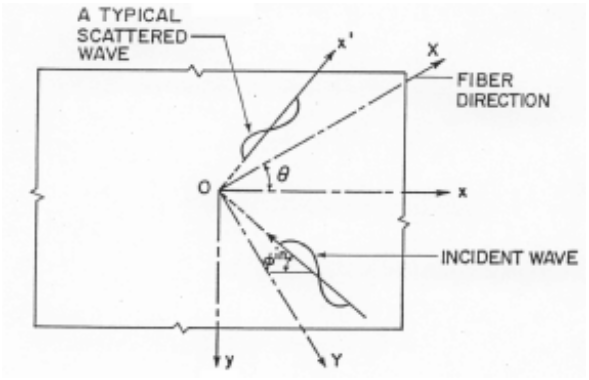


**Figure 2. Plan view of a typical lamina (layer) showing fibre orientation and wave normals**

### 2.2 *Solution for scattering problem*

The hybrid method described in [4,5] is adopted for solving this scattering problem. The hybrid method combines finite element formulation in a bounded interior region of the plate with a wave function expansion representation in the exterior region. The regions are connected along vertical boundaries $B^+$ at $x = x^+$, and $B^-$ at $x = x^-$ as shown in Figure 1. Let $\kappa$ be the wave number of the incident wave in the direction of propagation. Thus, $\kappa$ should be one of the admissible real roots of the dispersion equation for off-axis propagation. Since the flaw extends to infinity in y-direction, the scattered field must have the same wave number in the y-direction as the incident field. Thus, each of the scattered wave modes will have a constant wave number $\eta_0$ ( $= \kappa \text{ Sin } \phi^{in}$ ) in the negative y direction. Therefore, for time-harmonic waves, y and t variation can be factored out as

$$\begin{Bmatrix} u(x,y,z,t) \\ v(x,y,z,t) \\ w(x,y,z,t) \end{Bmatrix} = \begin{Bmatrix} \hat{u}(x,z) \\ \hat{v}(x,z) \\ \hat{w}(x,z) \end{Bmatrix} \exp[-j(\eta_0 y + \omega t)] \qquad (1)$$

where $\omega$ is the circular frequency and $j = \sqrt{-1}$ .

The procedure for finite element formulation for the interior region R is very similar to that for the plane strain case given in [4]. The finite element representation of the interior region should include singular elements at crack tips if the flaw considered is a crack or a delamination. The standard discretization process in the finite element method leads to

$$\delta\{\overline{q}\}^T [S]\{q\} - \delta\{\overline{q}_B\}^T \{P_B\} = 0 \qquad (2)$$

where

$$[S] = [K] - \omega^2[M] \tag{3}$$

in which: [K] and [M] are, respectively, the global stiffness and mass matrices of the interior region; {q} is the nodal displacement vector corresponding to interior nodes; and $\{q_B\}$ and $\{P_B\}$ are, respectively, the nodal displacement vector and the interaction force vector corresponding to the boundary nodes. δ implies first variation and overbar denotes complex conjugate.

The wave field in the exterior regions $R^+$ and $R^-$ is the superposition of those due to the incident wave and the scattered waves. Using the wave function expansion procedure, the scattered wave field can be expressed in terms of the wave functions (ie wave modes) supported by the free infinite composite plate with no flaws and the unknown reflected and transmitted wave amplitudes. The theoretical details of the methodology adopted to obtain wave functions can be found in our work reported in [6]. The procedure starts with dividing each layer into several sub-layers. The exact dispersion relation of the infinite plate is developed using the propagator matrices as

$$f(\omega, k) = 0 \tag{4}$$

where k denotes the x-direction wave number of a typical wave mode. It is well known that the plate wave modes are dispersive and at any given frequency ω, there are only a finite number of propagating modes that carry energy away from a source of excitation or upon scattering from an inhomogeneity or flaw. However, in order to satisfy the boundary conditions at the source or at a boundary of discontinuity it is necessary to include also the non-propagating modes in the modal representation of the displacement field. The wave numbers (k) for the propagating and non-propagating modes at a given frequency of excitation can be found by solving the dispersion equation (4) for the plate. For each wave number k, the corresponding displacement wave function (which is basically a vector containing x and z direction displacement at each sub-layer level) can be determined using the propagator matrix for each sub-layer. This has been discussed in the references cited above.

The solution to the scattering problem is obtained by imposing the continuity of total (incident plus scattered) displacements and tractions on the boundaries. This is achieved by substituting for $\{q_B\}$ and $\{P_B\}$ from the wave function expansion into equation (2). This leads to a system of linear equations to solve for the unknown reflected wave amplitudes ( $A_m^+$ ) and transmitted amplitudes ( $A_m^-$ ). These amplitudes are then used to obtain boundary nodal displacements and, in turn, to obtain interior nodal displacements. The reflection coefficient $R_{pm}$ of the m-th reflected mode and transmission coefficient $T_{pm}$ of the m-th transmitted mode, due to the p-th incident wave mode, are given by

$$R_{pm} = A_m^+ / A_p^{in}, \qquad T_{pm} = \begin{cases} A_m^- / A_p^{in} & \text{for } m \neq p \\ (A_p^{in} + A_m^-) / A_p^{in} & \text{for } m = p \end{cases} \tag{5}$$

in which, $A_p^{in}$ is the amplitude of the incident wave mode. At this stage, numerical solution of all displacement and stress components for the scattered field and, hence for total field, is fully defined. As the solution process involves numerous intricate computational steps, we are not quite sure whether the solution we have now is an acceptable one. One way of checking the accuracy of the numerical solution is to see whether it satisfies the elastodynamic reciprocity relations developed in the next section.

### 2.3 *Reciprocity relations*

The reciprocity relations are derived from the elastodynamic reciprocity theorem [7-8], which may be written using the usual tensor notation, in the absence of body forces, as

$$\oint_S (u_j^B \sigma_{jk}^A - u_j^A \sigma_{jk}^B) n_k \, dS = 0, \qquad j,k = x,y,z \tag{6}$$

where $u_j^A$ and $\sigma_{jk}^A$ represent the displacements and stresses corresponding to elastodynamic state A while $u_j^B$ and $\sigma_{jk}^B$ are the displacements and stresses corresponding to elastodynamic state B, in a region V bounded by a surface S. Wave fields corresponding to both elastodynamic states vary harmonically in time with circular frequency $\omega$. When writing equation (6), Einstein's summation convention of repeated indices has been assumed to hold, and the displacement components u, v, w have been represented by $u_x$, $u_y$, $u_z$, respectively. In order to derive the reciprocity relations, the orthogonality relations among the wave modes have to be established first.

For convenience in derivation of orthogonality relations, few notations are introduced first. Let the wave number pair $(k_n,\zeta_0)$ denote an admissible wave mode propagating in the first quadrant of x-y plane in an infinite composite plate with no flaws. Herein, $k_n$ represents the positive x direction wave number and $\zeta_0$ (which is fixed) represents the positive y direction wave number as opposed to the definition of $\eta_0$ in equation (1). Note that $\eta_0 = -\zeta_0$. In a similar manner, let the wave number pairs $(-k_n^*,\zeta_0)$, $(-k_n,-\zeta_0)$, and $(k_n^*,-\zeta_0)$ denote the wave modes corresponding to second, third and fourth quadrants of the x-y plane, respectively. It should be mentioned here that if $(k_n,\zeta_0)$-th wave mode is an admissible wave mode (of the dispersion relation of the plate), then $(-k_n,-\zeta_0)$-th wave mode, which is propagating in the opposite direction, is also an admissible wave mode. Similarly, if $(k_n^*,-\zeta_0)$-th wave mode is admissible, then $(-k_n^*,\zeta_0)$-th wave mode is also admissible. This point can be explained by visualising the configuration of the plate with respect to a new coordinate system that is obtained after rotating the x,y axes by $180^0$ about the z axis. However, when $(k_n,\zeta_0)$-th wave mode is an admissible wave mode, $(k_n,-\zeta_0)$-th wave mode is not necessarily an admissible wave mode. Due to this reason, a

superscript star ($^*$) has been introduced to the x-direction wave numbers of wave modes corresponding to second and fourth quadrants of the x-y plane. Note that $(k_n,-\zeta_0)$-th wave mode is admissible when the fibers in each layer are aligned either in x or y directions. This can be visualised by considering the mirror image of the plate with respect to the x-z plane.

The orthogonality relations are derived by applying the reciprocity theorem to the close region V bounded by planes z = 0, z = H, $x = x_1$, $x = x_2$, $y = y_1$, and $y = y_2$ where $x_1$, $x_2$, $y_1$ and $y_2$ are coordinates chosen in such a way that $x_2 > x_1$ and $y_2 > y_1$. State A is taken to be the field due to $(-k_n^*, \zeta_0)$-th wave mode and state B is taken to be the field due to $(k_m^*, -\zeta_0)$-th wave mode. Then, the wave fields due to two states can be written as

$$u_j^A \rightarrow A_{-n}^{*+}\{u_{-n}^{*+}\}\exp[j(-k_n^* x + \zeta_0 y)] \tag{7a}$$

$$\sigma_{jk}^A \rightarrow A_{-n}^{*+}\begin{Bmatrix}\{\sigma_{-nx}^{*+}\}\\ \{\sigma_{-ny}^{*+}\}\end{Bmatrix}\exp[j(-k_n^* x + \zeta_0 y)] \tag{7b}$$

$$u_j^B \rightarrow A_m^{*-}\{u_m^{*-}\}\exp[j(k_m^* x - \zeta_0 y)] \tag{7c}$$

$$\sigma_{jk}^B \rightarrow A_m^{*-}\begin{Bmatrix}\{\sigma_{mx}^{*-}\}\\ \{\sigma_{my}^{*-}\}\end{Bmatrix}\exp[j(k_m^* x - \zeta_0 y)] \tag{7d}$$

where $A_{-n}^{*+}$, $\{u_{-n}^{*+}\}$, $\{\sigma_{-nx}^{*+}\}$ and $\{\sigma_{-ny}^{*+}\}$ represent the amplitude, displacement mode shape vector, mode shape vector of tractions on x face and the mode shape vector of tractions on y face, respectively, for the $(-k_n^*, \zeta_0)$-th wave mode; and $A_m^{*-}$, $\{u_m^{*-}\}$, $\{\sigma_{mx}^{*-}\}$ and $\{\sigma_{my}^{*-}\}$ represent the same quantities for the $(k_m^*, -\zeta_0)$-th wave mode. Application of the elastodynamic reciprocity theorem expressed in mathematical form in equation (6) to the region V for states A and B defined in equations (7) results in

$$\{\exp[j(k_m^* - k_n^*)x_2] - \exp[j(k_m^* - k_n^*)x_1]\}\, I[(k_m^*, -\zeta_0);(-k_n^*, \zeta_0)] = 0 \tag{8}$$

where the notation $I[(k_m^*, -\zeta_0);(-k_n^*, \zeta_0)]$ has been used to represent the integral

$$\int_0^H (\{u_m^{*-}\}^T\{\sigma_{-nx}^{*+}\} - \{u_{-n}^{*+}\}^T\{\sigma_{mx}^{*-}\})dz.$$

Since $x_1$ and $x_2$ are arbitrary, equation (8) leads to the orthogonality relation

$$I[(k_m^*,-\zeta_0);(-k_n^*,\zeta_0)] = 0 \quad \text{for} \quad k_m^* \neq k_n^*. \tag{9}$$

It should be noted that the net contributions from the surface integrals in equation (6) on planes $y = y_1$ and $y = y_2$ amount to zero.

In a similar manner, choosing states A and B as the fields due to $(k_n,\zeta_0)$-th and $(-k_m,-\zeta_0)$-th wave modes, respectively, it can be shown that

$$I[(-k_m,-\zeta_0);(k_n,\zeta_0)] = 0 \quad \text{for} \quad k_m \neq k_n. \tag{10}$$

Adopting a similar approach, the following orthogonality relations can be derived:

$$I[(k_m^*,-\zeta_0);(k_n,\zeta_0)] = 0, \tag{11}$$

$$I[(-k_m,-\zeta_0);(-k_n^*,\zeta_0)] = 0. \tag{12}$$

In order to derive reciprocity relations, region V is chosen as the region of the plate surrounding the flaw, bounded by the planar surfaces $z = 0$, $z = H$, $x = x_3$ $(x_3 \geq x^+)$, $x = x_4$ $(x_4 \leq x^-)$, $y = y_1$, and $y = y_2$ (where $y_1$ and $y_2$ are arbitrary, and $y_2 > y_1$). The reciprocity relations among the reflection coefficients can be derived from equation (6) by choosing state A as the total field due to $(-k_n,-\zeta_0)$-th incident wave mode and state B as the total field due to $(k_p^*,\zeta_0)$-th incident wave mode. Let $R_{nq}$ and $T_{nq}$ denote the reflection and transmission coefficients, respectively, due to $(-k_n,-\zeta_0)$-th incident wave mode; and $R_{pm}^*$ and $T_{pm}^*$ denote the same quantities due to $(-k_p^*,\zeta_0)$-th incident wave mode. In view of the orthogonality relations given in equations (9) to (12), the reciprocity relations becomes (after some algebraic manipulations)

$$R_{pn}^* \varsigma_n = R_{np} \varsigma_p^* \tag{13}$$

where

$$\varsigma_n = \int_0^H (\{u_n^+\}^T \{\sigma_{-nx}^-\} - \{u_{-n}^-\}^T \{\sigma_{nx}^+\}) dz, \tag{14a}$$

$$\varsigma_p^* = \int_0^H (\{u_p^{*-}\}^T \{\sigma_{-px}^{*-}\} - \{u_{-p}^{*+}\}^T \{\sigma_{px}^{*-}\}) dz. \tag{14b}$$

In equation (14), $\{u_n^+\}$, $\{u_{-n}^-\}$, $\{u_p^{*-}\}$ and $\{u_{-p}^{*+}\}$ denote the displacement mode shape vectors corresponding to ($k_n$,$\zeta_0$)-th, ($-k_n$,-$\zeta_0$)-th, ($k_p^*$,-$\zeta_0$)-th and (-$k_p^*$,$\zeta_0$)-th wave modes, respectively, in an infinite plate with no flaw. The corresponding traction mode shape vectors on the x face are denoted by $\{\sigma_{nx}^+\}$, $\{\sigma_{-nx}^-\}$, $\{\sigma_{px}^{*-}\}$ and $\{\sigma_{-px}^{*-}\}$. It should be noted that the net contributions to the surface integral in equation (6) from surfaces $y = y_1$ and $y = y_2$ becomes zero.

Applying the reciprocity theorem to the same region V, with state A as the total field due to ($k_n$,$\zeta_0$)-th incident mode and state B as the total field due to (-$k_p$,-$\zeta_0$)-th incident mode, the reciprocity relation among the transmission coefficients can be derived as

$$T_{pn}\varsigma_n = T_{np}\varsigma_p \tag{15}$$

where $\varsigma_p$ is given by equation (14a) with n replaced by p. When deriving equation (15), it has been assumed that the flaw geometry is symmetric with respect to the x = 0 plane. It can be shown that, when the fibers in each layer are either in x or y direction, the reciprocity relation in equation (13) degenerates into

$$R_{pn}\varsigma_n = R_{np}\varsigma_p \ . \tag{16}$$

It is well known that scattered field consists of both propagating and evanescent (or non-propagating) wave modes. Wave numbers corresponding to propagating modes have only a real part whereas wave numbers of evanescent modes are in general complex numbers. Reflected and transmitted energies are carried only by the propagating modes. The time-averaged value of the energy flux associated with the n-th reflected propagating mode through the plate cross section due to ($-k_p$,-$\zeta_0$)-th incident propagating wave mode is given by

$$I_{pn}^+ = \frac{1}{2}\omega\,|A_p^{in}|^2\,|R_{pn}|^2\,(-j\varsigma_n)\,, \qquad 1 \le n \le N_{pr} \tag{17}$$

where $N_{pr}$ is the number of propagating wave modes in the reflected wave field. For more information on derivation details of equation (17), reader is referred to [4]. In a similar manner, the energy flux of the n-th transmitted propagating wave mode and the incident wave mode can be written, respectively, as

$$I_{pn}^- = \frac{1}{2}\omega\,|A_p^{in}|^2\,|T_{pn}|^2\,(-j\varsigma_n)\,, \qquad 1 \le n \le N_{pr} \tag{18}$$

$$I_p^{in} = \frac{1}{2}\omega \,|\, A_p^{in} \,|^2 \;\; (-j\varsigma_p)\,. \tag{19}$$

Let $E_{pn}^{-}$ be the proportion of energy of the $(-k_p, -\zeta_0)$-th incident propagating wave mode transferred into the n-th transmitted propagating mode during the scattering process. Then

$$E_{pn}^{-} = \frac{I_{pn}^{-}}{I_p^{in}} = |\, T_{pn} \,|^2 \, \frac{\varsigma_n}{\varsigma_p}. \tag{20}$$

Similarly, if the incident wave mode is the $(-k_n, -\zeta_0)$-th propagating mode, then the proportion of energy transferred into the p-th transmitted propagating mode can be expressed as

$$E_{np}^{-} = \frac{I_{np}^{-}}{I_n^{in}} = |\, T_{np} \,|^2 \, \frac{\varsigma_p}{\varsigma_n}. \tag{21}$$

In view of equations (20) and (21), the reciprocity relation (15) for transmitted wave simplifies to

$$E_{pn}^{-} = E_{np}^{-} \quad \text{for arbitrary fibre directions in layers.} \tag{22}$$

Following a similar procedure, it can be shown that, for the reflected waves , the reciprocity relation in equation (16) reduces to

$$E_{pn}^{+} = E_{np}^{+} \quad \text{when fibres in layers are aligned with global x,y directions.} \tag{23}$$

It is clear from equations (20) and (21) that, for the numerical computation of energy proportions, we need to evaluate $\varsigma_n$ in equation (14a). $\{u_n^+\}$ and $\{\sigma_{nx}^+\}$ in equation (14a) can be expressed in components form, respectively, as

$$\{u_n^+\} = \begin{Bmatrix} u_{xn}^+ \\ u_{yn}^+ \\ u_{zn}^+ \end{Bmatrix}, \quad \text{and} \qquad \{\sigma_{nx}^+\} = \begin{Bmatrix} \sigma_{xxn}^+ \\ \sigma_{xyn}^+ \\ \sigma_{xzn}^+ \end{Bmatrix}. \tag{24}$$

Then, it can be shown that $\{u_{-n}^-\}$ and $\{\sigma_{-nx}^-\}$ are given by

$$\{u_{-n}^-\} = \begin{Bmatrix} -u_{xn}^+ \\ -u_{yn}^+ \\ u_{zn}^+ \end{Bmatrix}, \quad \text{and} \quad \{\sigma_{-nx}^-\} = \begin{Bmatrix} \sigma_{xxn}^+ \\ \sigma_{xyn}^+ \\ -\sigma_{xzn}^+ \end{Bmatrix}. \tag{25}$$

In view of equations (24) and (25), $\varsigma_n$ reduces to

$$\varsigma_n = 2\int_0^H \{u_n^+\}^T \{\sigma_{-nx}^-\} dz . \tag{26}$$

After the dispersion relation in equation (4) is solved for a given $\omega$, the components of the displacement wave function $\{u_{-n}^-\}$ and stress wave function $\{\sigma_{-nx}^-\}$ for wave mode n at each sublayer interface can be determined using the propagator matrices. Then the integral in equation (26) can be approximated as

$$\varsigma_n = -2\{F_n\}^T \{q_n\}, \tag{27}$$

where $\{q_n\}$ is a displacement vector constructed from the displacement components at each sublayer interface and $\{F_n\}$ is a force vector constructed using the stress components at each sublayer interface. Now energy proportion terms in equations (20) to (23) are fully defined and can be evaluated numerically using the scattering solution results.

## 3 Results and discussion

The simplified reciprocity relations derived in the previous section has been used to check the accuracy of four example scattering problems described below:

*Example 1*: Scattering by a thin symmetric normal edge crack in a uni-directional fiber-reinforced homogeneous graphite-epoxy plate. The geometry of the crack is as shown in Figure 3a.

*Example 2* : Scattering by a thin symmetric normal edge crack in an 8 layer graphite-epoxy plate with the stacking sequence of $0^0/90^0/0^0/90^0/90^0/0^0/90^0/0^0$ . The geometry of the crack is same as that shown in Figure 3a.

*Example 3* : Scattering by a thin crack located at the fixed-end of a homogeneous isotropic plate shown in Figure 3b.

*Example 4* : Scattering by a thin crack located at the fixed-end of a uni-directional fiber-reinforced homogeneous graphite-epoxy plate. The geometry of the crack is same as that shown in Figure 3b.

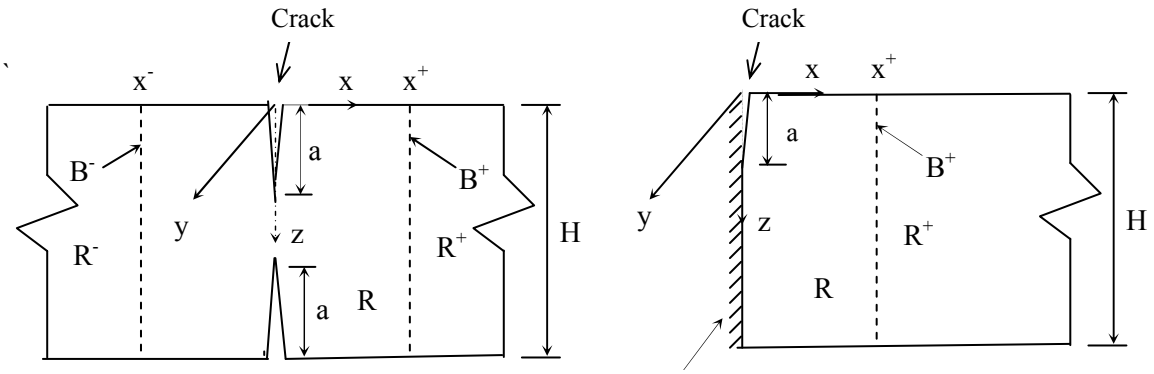


(a) Symmetric normal edge crack (b) Fixed end crack

**Figure 3. Geometry of the flaws for example problems**

The graphite-epoxy composite material in each layer of plates in Examples 1, 2 and 4 are considered to be transversely isotropic. The elastic constants ($C_{ij}$) for the transversely isotropic graphite-epoxy composite material are given in Table 1. More information on $C_{ij}$ constants and their relation to the stiffness matrix in equation (3), and the procedure for their transformation from fiber direction to global x,y directions can be found in [9]. The Poisson's ratio for the isotropic material in Example 3 is taken to be 0.25.

**Table 1: Elastic constants of graphite-epoxy lamina (in GPa)**

| Lamina | $C_{11}$ | $C_{33}$ | $C_{13}$ | $C_{55}$ |
|---|---|---|---|---|
| $0^0$ | 160.73 | 13.92 | 6.44 | 7.07 |
| $90^0$ | 13.92 | 13.92 | 6.92 | 3.50 |

Numerical results from the hybrid method for the magnitudes of the reflection and the transmission coefficients ($|R_{pn}|$ and $|T_{pn}|$), and proportions of the reflected and the transmitted energies ($E^{+}_{pn}$ and $E^{-}_{pn}$) for example 1 are presented in Table 2. The results correspond to a normalized frequency $\Omega$ ($=\omega H/(2\sqrt{(C_{55}/\rho)_0})$ where $\rho$ is the density of the graphite-epoxy composite) of 2.0 and a normalized crack length (= a/(0.5H)) of 0.1 or 0.5 as given in the table. In this table, p and n denote the incident and the scattered wave mode numbers, respectively, and all the incident modes considered are symmetric modes. Note that, due to the symmetry of the problem with respect to the mid-plane of the plate, the scattered wave field consists of only symmetric or anti-symmetric modes depending on whether the incident mode is a symmetric or an anti-symmetric one. It can be seen from this table that final form of the reciprocity relations among the proportions of energy as given in equations (22) and (23) are satisfied with negligible errors. Also, it is seen that some reflection and transmission

coefficients are quite sensitive to the orientation and the depth of the crack, and the incident wave mode number. Although not shown here, our computations showed that coefficients are also sensitive to the incident mode frequency. Satisfaction of reciprocity relations can be taken as an indication of the accuracy of the scattering results.

Table 3 shows the scattering results for the 8 layer composite plate in Example 2 at a normalized frequency of 4 and at a normalized crack length of 0.5. Frequency normalisation factor for this example is same as that for Example 1. It is clearly seen that reciprocity relations in equations (22) and (23) are satisfied with negligible errors.

**Table 2: Scattering results for Example 1 when Ω=2**

**(a) $\theta = 0^0$, $\varphi^{in} = 45^0$, $\eta_0 = 1.440$**

| p | $k_p$ | a/(0.5H) | n | $E^+_{pn}$ | $E^-_{pn}$ | $\lvert R_{pn}\rvert$ | $\lvert T_{pn}\rvert$ |
|---|---|---|---|---|---|---|---|
| 1 | 1.440 | 0.1 | 1 | 0.002 | 0.993 | 0.044 | 0.996 |
| | | | 2 | 0.001 | 0.001 | 0.051 | 0.048 |
| | | 0.5 | 1 | 0.009 | 0.821 | 0.095 | 0.906 |
| | | | 2 | 0.127 | 0.042 | 0.718 | 0.409 |
| 2 | 0.324 | 0.1 | 1 | 0.001 | 0.001 | 0.012 | 0.012 |
| | | | 2 | 0.000 | 0.999 | 0.011 | 0.999 |
| | | 0.5 | 1 | 0.128 | 0.041 | 0.178 | 0.101 |
| | | | 2 | 0.070 | 0.760 | 0.264 | 0.872 |

**(b) $\theta = 22.5^0$, $\varphi^{in} = 22.5^0$, $\eta_0 = 0.780$**

| p | $k_p$ | a/(0.5H) | n | $E^+_{pn}$ | $E^-_{pn}$ | $\lvert R_{pn}\rvert$ | $\lvert T_{pn}\rvert$ |
|---|---|---|---|---|---|---|---|
| 1 | 1.882 | 0.1 | 1 | 0.000 | 0.998 | 0.009 | 0.999 |
| | | | 2 | 0.000 | 0.000 | 0.062 | 0.033 |
| | | 0.5 | 1 | 0.002 | 0.833 | 0.105 | 0.913 |
| | | | 2 | 0.081 | 0.082 | 1.357 | 0.632 |
| 2 | 0.813 | 0.1 | 1 | 0.000 | 0.000 | 0.014 | 0.007 |
| | | | 2 | 0.000 | 1.000 | 0.009 | 1.000 |
| | | 0.5 | 1 | 0.000 | 0.082 | 0.024 | 0.129 |
| | | | 2 | 0.075 | 0.842 | 0.590 | 0.918 |

Note: p and n denote the incident and scattered wave mode numbers, respectively. Symmetric incident wave modes have been considered.

**Table 3: Scattering results for Example 2 when Ω=4, a/(0.5H)=0.5, θ for $0^0$ lamina = $0^0$, $\varphi^{in} = 45^0$ , and $\eta_0 = 3.362$**

| p | $k_p$ | n | $E^+_{pn}$ | $E^-_{pn}$ | $\lvert R_{pn}\rvert$ | $\lvert T_{pn}\rvert$ |
|---|---|---|---|---|---|---|
| 1 | 3.362 | 1 | 0.706 | 0.180 | 0.840 | 0.424 |
| | | 2 | 0.007 | 0.108 | 0.143 | 0.571 |
| 2 | 0.662 | 1 | 0.007 | 0.108 | 0.047 | 0.189 |
| | | 2 | 0.543 | 0.340 | 0.737 | 0.583 |

Proportions of reflected energy for scattering by the fixed end crack shown Figure 2b are reported in Table 4 and 5. Table 4 is for the isotropic plate (Example 3) and Table 5 is for a uni-axially fibre-reinforced plate (Example 4). Note that minor modifications to the theory presented in the previous section is required for this problem as the exterior region has only one region which consists of the reflected wave field. The reciprocity relation in equation (22) does not apply for this fixed end crack scattering problem as there is no transmitted field. The reciprocity relation for the reflected wave modes is given by equation (23).

For Example 3, the results in Table 4 correspond to a normalised frequency Ω ($=\omega H/(2\sqrt{\mu/\rho}$ ) where $\rho$ is the density and $\mu$ is the shear modulus of the plate) of $3.5\sqrt{3}$. Five different crack lengths have been considered. At this frequency ($\Omega = 3.5\sqrt{3}$ ), the dispersion relation in equation (4) has three symmetric propagating modes (denoted as 1S, 2S and 3S in Table 4) and four anti-symmetric modes (usually denoted as 1A, 2A, 3A and 4A). It is seen from Table 4 that reciprocity relations among the reflected modes as given in equation (23) are satisfied with reasonable accuracy for the five different crack lengths considered. In this table, a normalized crack length of 0.0 and 2.0 represent, respectively, the full reflection by a fixed end and reflection by a free end (i.e. a crack right through the full thickness of the plate).

**Table 4: Reflected energy proportions $E^+_{pn}$ for Example 3 for different crack lengths when $\Omega = 3.5\sqrt{3}$ , θ = $0^0$, $\varphi^{in} = 0^0$ , $\eta_0 = 0$**

| p, n | $E^+_{pn}$ | a/(0.5H) | | | | |
|---|---|---|---|---|---|---|
| | | 0.0 | 0.5 | 1.0 | 1.5 | 2.0 |
| p=1=1S, n=2=2S | $E^+_{12}$ | 0.034 | 0.075 | 0.035 | 0.089 | 0.109 |
| P=2=2S, n=1=1S | $E^+_{21}$ | 0.035 | 0.075 | 0.035 | 0.089 | 0.109 |
| p=1=1S, n=3=3S | $E^+_{13}$ | 0.230 | 0.083 | 0.059 | 0.039 | 0.304 |
| P=3=3S, n=1=1S | $E^+_{31}$ | 0.230 | 0.083 | 0.059 | 0.039 | 0.303 |
| p=1=1S, n=4=1A | $E^+_{14}$ | 0.000 | 0.353 | 0.170 | 0.079 | 0.000 |
| P=4=1A, n=1=1S | $E^+_{41}$ | 0.000 | 0.354 | 0.171 | 0.081 | 0.000 |

| | | | | | | |
|---|---|---|---|---|---|---|
| p=1=1S, n=5=2A | $E^{+}_{15}$ | 0.000 | 0.030 | 0.090 | 0.074 | 0.000 |
| P=5=2A, n=1=1S | $E^{+}_{51}$ | 0.000 | 0.030 | 0.090 | 0.075 | 0.000 |
| p=1=1S, n=6=3A | $E^{+}_{16}$ | 0.000 | 0.129 | 0.167 | 0.213 | 0.000 |
| P=6=3A, n=1=1S | $E^{+}_{61}$ | 0.000 | 0.129 | 0.168 | 0.213 | 0.000 |
| p=1=1S, n=7=4A | $E^{+}_{17}$ | 0.000 | 0.202 | 0.368 | 0.275 | 0.000 |
| P=7=4A, n=1=1S | $E^{+}_{71}$ | 0.000 | 0.203 | 0.369 | 0.277 | 0.000 |
| p=2=2S, n=3=3S | $E^{+}_{23}$ | 0.043 | 0.053 | 0.104 | 0.112 | 0.022 |
| P=3=3S, n=2=2S | $E^{+}_{32}$ | 0.043 | 0.054 | 0.105 | 0.113 | 0.022 |
| p=2=2S, n=4=1A | $E^{+}_{24}$ | 0.000 | 0.126 | 0.004 | 0.013 | 0.000 |
| P=4=1A, n=2=2S | $E^{+}_{42}$ | 0.000 | 0.126 | 0.005 | 0.014 | 0.000 |
| p=2=2S, n=5=2A | $E^{+}_{25}$ | 0.000 | 0.079 | 0.057 | 0.070 | 0.000 |
| P=5=2A, n=2=2S | $E^{+}_{52}$ | 0.000 | 0.079 | 0.057 | 0.070 | 0.000 |
| p=2=2S, n=6=3A | $E^{+}_{26}$ | 0.000 | 0.622 | 0.698 | 0.516 | 0.000 |
| P=6=3A, n=2=2S | $E^{+}_{62}$ | 0.000 | 0.621 | 0.698 | 0.516 | 0.000 |
| p=2=2S, n=7=4A | $E^{+}_{27}$ | 0.000 | 0.018 | 0.080 | 0.075 | 0.000 |
| P=7=4A, n=2=2S | $E^{+}_{72}$ | 0.000 | 0.018 | 0.080 | 0.075 | 0.000 |
| p=3=3S, n=4=1A | $E^{+}_{34}$ | 0.000 | 0.027 | 0.006 | 0.032 | 0.000 |
| P=4=1A, n=3=3S | $E^{+}_{43}$ | 0.000 | 0.027 | 0.006 | 0.032 | 0.000 |
| p=3=3S, n=5=2A | $E^{+}_{35}$ | 0.000 | 0.015 | 0.366 | 0.019 | 0.000 |
| P=5=2A, n=3=3S | $E^{+}_{53}$ | 0.000 | 0.015 | 0.364 | 0.019 | 0.000 |
| p=3=3S, n=6=3A | $E^{+}_{36}$ | 0.000 | 0.068 | 0.020 | 0.094 | 0.000 |
| P=6=3A, n=3=3S | $E^{+}_{63}$ | 0.000 | 0.067 | 0.019 | 0.093 | 0.000 |
| p=3=3S, n=7=4A | $E^{+}_{37}$ | 0.000 | 0.007 | 0.187 | 0.008 | 0.000 |
| P=7=4A, n=3=3S | $E^{+}_{73}$ | 0.000 | 0.007 | 0.187 | 0.008 | 0.000 |
| p=4=1A, n=5=2A | $E^{+}_{45}$ | 0.063 | 0.136 | 0.244 | 0.407 | 0.069 |
| P=5=2A, n=4=1A | $E^{+}_{54}$ | 0.063 | 0.136 | 0.245 | 0.407 | 0.070 |
| p=4=1A, n=6=3A | $E^{+}_{46}$ | 0.051 | 0.020 | 0.074 | 0.165 | 0.348 |
| P=6=3A, n=4=1A | $E^{+}_{64}$ | 0.051 | 0.020 | 0.074 | 0.163 | 0.348 |
| p=4=1A, n=7=4A | $E^{+}_{47}$ | 0.132 | 0.010 | 0.169 | 0.181 | 0.093 |
| P=7=4A, n=4=1A | $E^{+}_{74}$ | 0.133 | 0.010 | 0.169 | 0.178 | 0.093 |
| p=5=2A, n=6=3A | $E^{+}_{56}$ | 0.159 | 0.039 | 0.011 | 0.002 | 0.017 |
| P=6=3A, n=5=2A | $E^{+}_{65}$ | 0.158 | 0.039 | 0.011 | 0.002 | 0.017 |
| p=5=2A, n=7=4A | $E^{+}_{57}$ | 0.766 | 0.568 | 0.084 | 0.425 | 0.900 |
| P=7=4A, n=5=2A | $E^{+}_{75}$ | 0.766 | 0.568 | 0.083 | 0.421 | 0.897 |
| p=6=3A, n=7=4A | $E^{+}_{67}$ | 0.077 | 0.116 | 0.026 | 0.012 | 0.005 |
| P=7=4A, n=6=3A | $E^{+}_{76}$ | 0.078 | 0.116 | 0.026 | 0.013 | 0.005 |

Note: S and A denote symmetric and anti-symmetric modes, respectively.

For Example 4, the results in Table 5 correspond to a normalised frequency Ω of 6.0. Frequency normalisation factor for this example is same as that for Example 1. As in Example 3, five different crack lengths have been considered. At Ω equal to 6.0, the dispersion relation for the uni-axially fiber-reinforced plate has three symmetric propagating modes (denoted as 1S, 2S and 3S in Table 5) and four anti-symmetric modes (denoted as 1A, 2A, 3A and 4A). As in previous example scattering

problems considered in this paper, it is seen from Table 5 that reciprocity relations among the proportions of energy in reflected modes are satisfied with reasonable accuracy for all crack lengths considered.

**Table 5: Reflected energy proportions $E^{+}_{pn}$ for Example 4 for different crack lengths when $\Omega$=6.0, $\theta = 0^0$, $\varphi^{in} = 0^0$, $\eta_0 = 0$**

| p, n | $E^{+}_{pn}$ | a/(0.5H) | | | | |
|---|---|---|---|---|---|---|
| | | 0.0 | 0.5 | 1.0 | 1.5 | 2.0 |
| p=1=1S, n=2=2S | $E^{+}_{12}$ | 0.000 | 0.033 | 0.001 | 0.013 | 0.014 |
| P=2=2S, n=1=1S | $E^{+}_{21}$ | 0.000 | 0.032 | 0.001 | 0.014 | 0.014 |
| p=1=1S, n=3=3S | $E^{+}_{13}$ | 0.014 | 0.001 | 0.038 | 0.006 | 0.219 |
| P=3=3S, n=1=1S | $E^{+}_{31}$ | 0.014 | 0.001 | 0.040 | 0.006 | 0.224 |
| p=1=1S, n=4=1A | $E^{+}_{14}$ | 0.000 | 0.556 | 0.567 | 0.506 | 0.000 |
| P=4=1A, n=1=1S | $E^{+}_{41}$ | 0.000 | 0.556 | 0.557 | 0.513 | 0.000 |
| p=1=1S, n=5=2A | $E^{+}_{15}$ | 0.000 | 0.288 | 0.170 | 0.174 | 0.000 |
| P=5=2A, n=1=1S | $E^{+}_{51}$ | 0.000 | 0.283 | 0.176 | 0.173 | 0.000 |
| p=1=1S, n=6=3A | $E^{+}_{16}$ | 0.000 | 0.023 | 0.004 | 0.020 | 0.000 |
| P=6=3A, n=1=1S | $E^{+}_{61}$ | 0.000 | 0.024 | 0.004 | 0.021 | 0.000 |
| p=1=1S, n=7=4A | $E^{+}_{17}$ | 0.000 | 0.050 | 0.158 | 0.226 | 0.000 |
| P=7=4A, n=1=1S | $E^{+}_{71}$ | 0.000 | 0.051 | 0.163 | 0.230 | 0.000 |
| p=2=2S, n=3=3S | $E^{+}_{23}$ | 0.004 | 0.151 | 0.006 | 0.138 | 0.009 |
| P=3=3S, n=2=2S | $E^{+}_{32}$ | 0.004 | 0.150 | 0.006 | 0.137 | 0.009 |
| p=2=2S, n=4=1A | $E^{+}_{24}$ | 0.000 | 0.020 | 0.006 | 0.016 | 0.000 |
| P=4=1A, n=2=2S | $E^{+}_{42}$ | 0.000 | 0.020 | 0.006 | 0.016 | 0.000 |
| p=2=2S, n=5=2A | $E^{+}_{25}$ | 0.000 | 0.004 | 0.027 | 0.007 | 0.000 |
| P=5=2A, n=2=2S | $E^{+}_{52}$ | 0.000 | 0.004 | 0.027 | 0.007 | 0.000 |
| p=2=2S, n=6=3A | $E^{+}_{26}$ | 0.000 | 0.631 | 0.916 | 0.729 | 0.000 |
| P=6=3A, n=2=2S | $E^{+}_{62}$ | 0.000 | 0.631 | 0.916 | 0.728 | 0.000 |
| p=2=2S, n=7=4A | $E^{+}_{27}$ | 0.000 | 0.078 | 0.044 | 0.049 | 0.000 |
| P=7=4A, n=2=2S | $E^{+}_{72}$ | 0.000 | 0.078 | 0.044 | 0.048 | 0.000 |
| p=3=3S, n=4=1A | $E^{+}_{34}$ | 0.000 | 0.018 | 0.019 | 0.026 | 0.000 |
| P=4=1A, n=3=3S | $E^{+}_{43}$ | 0.000 | 0.017 | 0.017 | 0.027 | 0.000 |
| p=3=3S, n=5=2A | $E^{+}_{35}$ | 0.000 | 0.006 | 0.213 | 0.011 | 0.000 |
| P=5=2A, n=3=3S | $E^{+}_{53}$ | 0.000 | 0.006 | 0.212 | 0.011 | 0.000 |
| p=3=3S, n=6=3A | $E^{+}_{36}$ | 0.000 | 0.188 | 0.055 | 0.147 | 0.000 |
| P=6=3A, n=3=3S | $E^{+}_{63}$ | 0.000 | 0.189 | 0.056 | 0.148 | 0.000 |
| p=3=3S, n=7=4A | $E^{+}_{37}$ | 0.000 | 0.027 | 0.598 | 0.021 | 0.000 |
| P=7=4A, n=3=3S | $E^{+}_{73}$ | 0.000 | 0.027 | 0.596 | 0.021 | 0.000 |
| p=4=1A, n=5=2A | $E^{+}_{45}$ | 0.003 | 0.219 | 0.266 | 0.280 | 0.029 |
| P=5=2A, n=4=1A | $E^{+}_{54}$ | 0.003 | 0.218 | 0.267 | 0.278 | 0.029 |
| p=4=1A, n=6=3A | $E^{+}_{46}$ | 0.001 | 0.010 | 0.015 | 0.009 | 0.054 |
| P=6=3A, n=4=1A | $E^{+}_{64}$ | 0.001 | 0.010 | 0.015 | 0.009 | 0.054 |
| p=4=1A, n=7=4A | $E^{+}_{47}$ | 0.003 | 0.021 | 0.072 | 0.001 | 0.064 |
| P=7=4A, n=4=1A | $E^{+}_{74}$ | 0.003 | 0.021 | 0.075 | 0.001 | 0.064 |

| | | | | | | |
|---|---|---|---|---|---|---|
| p=5=2A, n=6=3A | $E^{+}_{56}$ | 0.026 | 0.041 | 0.009 | 0.043 | 0.016 |
| P=6=3A, n=5=2A | $E^{+}_{65}$ | 0.026 | 0.040 | 0.009 | 0.043 | 0.016 |
| p=5=2A, n=7=4A | $E^{+}_{57}$ | 0.049 | 0.020 | 0.119 | 0.387 | 0.451 |
| P=7=4A, n=5=2A | $E^{+}_{75}$ | 0.051 | 0.021 | 0.119 | 0.389 | 0.452 |
| p=6=3A, n=7=4A | $E^{+}_{67}$ | 0.000 | 0.093 | 0.000 | 0.046 | 0.000 |
| P=7=4A, n=6=3A | $E^{+}_{76}$ | 0.000 | 0.093 | 0.000 | 0.045 | 0.000 |

Note: S and A denote symmetric and anti-symmetric modes, respectively.

## 4 Conclusion

By using the classical elastodynamic reciprocity theorem, simplified forms of elastodynamic reciprocity relations applicable for guided wave scattering by flaws in fiber-reinforced composite plates have been developed in this work. These relations are useful when developing ultrasonic non-destructive assessment techniques for flaw characterisation in composite structures. A hybrid method combining the finite element method with a wave function expansion procedure has been used to solve the wave scattering problem. The derivation has been presented for a plate with an arbitrary stacking sequence where each ply can have an arbitrary fiber direction. As the scattered field is expressed in wave function expansion, an arbitrary number of layers and thickness can be studied without appreciable increase in computational time. Numerical results verifying the derived reciprocity relations have been presented for four example scattering problems – two of them involving scattering by a symmetric normal edge crack in a uni-directional fibre-reinforced composite plate and in an 8-layer cross-ply plate, and other two involving scattering by a fixed-end crack in an isotropic plate and in a uni-directional fibre-reinforced composite plate.

## 5 References


1. Bakis, C.E., Bank, L.C., Brown, V.L., Cosenza, E., Davalos, J.F., Lesko, J.J., Machida, A. Rizkalla, S.H. and Triantafillou, T.C., "Fiber-reinforced polymer composites for construction – state-of-the-art-Review". *Journal of Composites for Construction;* Vol. 6(2), 2002, pp. 73-87.
2. Chimenti, D. E., "Guided waves in plates and their use in material characterization". *Applied Mechanics Review;* Vol. 50, 1997, pp. 247-284.
3. Datta, S. K., "Wave propagation in composite plates and shells". *Comprehensive Composite Materials;* Vol. 1, 2000, Chapter 18.
4. Karunasena, W., shah, A.H. and Datta, S.K., "Plane strain wave scattering by cracks in laminated composite plates". *Journal of Engineering Mechanics, ASCE;* Vol. 117(8), 1991, 1738-1754.

5. Karunasena, W., "Numerical modelling of obliquely incident guided wave scattering by a crack in a laminated composite plate". *Proceedings of Structural Integrity and Fracture (SIF2004)*, Brisbane, Australia.
6. Karunasena, W, Shah, A H. and Datta, S K, "Reflection of plane strain waves at the free edge of a laminated composite plate". *International Journal of Solids and Structures*; Vol. 27(8), 1991, 949-964.
7. Achenbach, J.D., *Wave Propagation in Elastic Solids.* North Holland, Amsterdam, 1973.
8. Auld, B.A., *Acoustic Fields and Waves in Solids – Vol. 2*. Wiley-Interscience, New York, 1973.
9. Karunasena, W, Bratton, R.L, Shah, A H. and Datta, S K, "Elastic wave propagation in laminated composite plates". *Journal of Engineering Materials and Technology, ASME*; Vol. 113, 1991, 413-420.